Case Studies in Construction Materials 20 (2024) e03351

Contents lists available at ScienceDirect

Case Studies in Construction Materials

journal homepage: www.elsevier.com/locate/cscm

Effect of silica fume on the performance of high-early-strength UHPC prepared with magnesium ammonium phosphate cement

Zhi-hai He [a,b], Yuan-yuan Jiang [a], Jin-yan Shi [c,*], Jihui Qin [d], De-e Liu [e], Çağlar Yalçınkaya [f], Yi-feng He [a,g]

[a] College of Civil Engineering, Shaoxing University, Shaoxing 312000, China
[b] Key Laboratory of Rock Mechanics and Geohazards of Zhejiang Province, Shaoxing 312000, China
[c] School of Civil Engineering, Central South University, Changsha 410075, China
[d] Department of Civil, Architectural, and Environmental Engineering, Missouri University of Science and Technology, Rolla, MO 65401, USA
[e] School of Materials Science and Engineering, Tianjin Chengjian University, Tianjin 300384, China
[f] Department of Civil Engineering, Dokuz Eylül University, İzmir, Turkiye
[g] Advanced Technologies and Materials Institute in the Conservation of Historic and Cultural Cities, Shaoxing 312000, China

ARTICLE INFO

Keywords:
Ultra-high performance concrete
Magnesium ammonium phosphate cement
Silica fume
Strength
Microstructure

ABSTRACT

Although ultra-high performance concrete (UHPC) prepared from Portland cement has high long-term strength and durability, its early strength development is still can be enhanced for shortening the prefabrication period or using it as a rapid repair material. Therefore, magnesium ammonium phosphate cement ultra-high performance concrete (MAPC-UHPC) was prepared using magnesium ammonium phosphate cement (MAPC), sand, steel fiber, and silica fume (SF) in this study. The effects of replacing MAPC with SF (5%–15%) on the fluidity, strength, and microstructure of MAPC-UHPC were studied. The results showed that the spread diameter of the MAPC-UHPC mixture was greater than 200 mm, and the setting time was between 5.5 and 8.5 min. Meanwhile, the 6-h compressive strength of MAPC-UHPC was higher than 100 MPa and could reach about 140 MPa in 28 d. When the 5%–15% binder was replaced by SF, the MAPC-UHPC fluidity and setting time increased with the increase in SF content. When 5% SF was used, the 6-h and 28-d compressive strengths of MAPC-UHPC increased by 3.91% and 3.86%, respectively, compared with the plain sample. The addition of SF promoted the formation of struvite and refined the pore structure, which also increased the compactness of the microstructure.

1. Introduction

UHPC is a new type of cement-based composite material. Its dense microstructure enables it to have ultra-high strength, good toughness, and excellent durability [1–6]. To date, it has been applied in various special high-end fields, such as bridges, highways, airports, and marine engineering [7,8]. The very early-age strength development of UHPC can still be enhanced to promote the use of UHPC as a rapid repair material or decrease the time and energy cost of prefabricated UHPC elements [9]. To accelerate the hydration rate and improve the early-age strength, steam curing is usually used in the production of UHPC [10,11], but this further increases the

* Corresponding author.
E-mail address: jinyan.shi@csu.edu.cn (J.-y. Shi).

https://doi.org/10.1016/j.cscm.2024.e03351
Received 29 February 2024; Received in revised form 28 April 2024; Accepted 26 May 2024
Available online 28 May 2024
2214-5095/© 2024 The Authors. Published by Elsevier Ltd. This is an open access article under the CC BY-NC license (http://creativecommons.org/licenses/by-nc/4.0/).

energy consumption and time costs. For the reasons mentioned, it is necessary to develop cleaner and low-cost technical approaches to improve the early mechanical properties of UHPC.

Magnesium phosphate cement (MPC) has been the focus of many researchers because of its unique and outstanding properties [12]. MPC is prepared by the acid-base chemical reaction of magnesia and phosphate (mainly including $NH_4H_2PO_4$ and KH_2PO_4). MPC mainly includes two types of magnesium ammonium phosphate cement (MAPC) and magnesium potassium phosphate cement (MKPC). The main hydration products are struvite and struvite (-K), and the hydration reaction is shown in Eqs. (1 and 2). Compared with ordinary Portland cement, MPC has the advantages of fast setting and hardening, high early strength, and good volume stability [13–19], which makes it especially suitable for repair materials [20,21], radioactive waste solidification materials [22], and biomedical materials [23].

$$MgO + NH_4H_2PO_4 + 5H_2O \rightarrow MgNH_4PO_4{\cdot}6H_2O \text{ (struvite)} \quad (1)$$

$$MgO + KH_2PO_4 + 5H_2O \rightarrow MgKPO_4{\cdot}6H_2O \text{ (k-struvite)} \quad (2)$$

To expand the application of MPC, many researchers have conducted extensive research on MPC modification. Qin et al. [21] concluded that the 24-h compressive strength of MKPC paste containing silica fume (SF) instead of 10% MgO could reach 43.1 MPa, which is 21.8% higher than the plain sample. This was mainly because incorporating an appropriate amount of SF could refine the pore size of MKPC samples and make the microstructure more dense. Chen et al. [24] concluded that the addition of 50% fly ash effectively prolonged the setting time of MPC, and the 3-d compressive strength was 55 MPa and the 28-d strength was 75 MPa. Gao et al. [25] studied the effect of SF content on MAPC strength. The results showed that the addition of 2.5%, 5%, and 7.5% SF improved the strength of MAPC at different ages, and the addition of 5% SF had the best effect, with compressive strengths of 68.5, 87.8 and 108.5 MPa at 1 h, 7 d, and 90 d, respectively. This was mainly because the SF particles were finer and could fill the pores of the mortar and make the mortar dense. Meanwhile, the reactive SiO_2 in SF was reacting with the remaining MgO to form $MgSiO_3$, which increased the gel product content. Thereby greatly improving the mechanical properties of MAPC. Qin et al. [26] prepared a magnesium phosphate ultra-high performance concrete (MPC-UHPC) by using MPC. Compared with traditional UHPC, MPC-UHPC mixed with an appropriate amount of fly ash showed a lower shrinkage ratio and higher early strength, which is particularly suitable for repairing materials. Traditional UHPC is commonly prepared by SF, but the effect of SF on the performance of MPC-UHPC has rarely been reported.

In order to cope with the repair projects of concrete structures in harsh environments, researchers usually use high-temperature curing and electric curing to produce UHPC with high early strength [27]. This requires complex equipment and consumes a lot of energy. Meanwhile, some researchers also use accelerating admixture to increase the early strength of UHPC. Yang et al. used C-S-H seeds to accelerate the hydration reaction of Portland cement and found that the strength of UHPC was slightly improved [28]. After further using a small content of sulphoaluminate cement to replace Portland cement, the early strength of UHPC was significantly improved. Therefore, the use of new binders has become an effective way to prepare high-early-strength UHPC. Zhu et al. used Portland cement, sulfoaluminate cement and gypsum to prepare rapidly hardening UHPC for rapid underwater repair projects, and its 4-h compressive strength can reach 19–24 MPa [29]. Zhou et al. used sulfoluminate cement to prepare UHPC and added various accelerating admixtures to enhance the early strength of UHPC. For plain UHPC, its 4-h compressive strength can reach 22.1 MPa, and after adding accelerating admixture, it can reach a maximum of 41.2 MPa [30,31]. However, their early strength is not satisfactory, and further development of high-early-strength UHPC is necessary.

Based on this, MAPC-UHPC was prepared using MAPC, and the effect of SF on the compressive strength, fluidity, and setting time of MAPC-UHPC was studied. Meanwhile, XRD, TG, SEM, and BET microscopic testing techniques were used to analyze the influence mechanism, which is conducive to expanding the research and application of UHPC.

2. Materials and methods

2.1. Raw materials

The dead burned magnesia (MgO) used in this test was provided by Huanai Magnesium Industry in Jiangsu, China. MgO is made from magnesite by calcining and grinding at 1750 ℃. Industrial grade ammonium dihydrogen phosphate (ADP) is a white columnar crystal provided by China Guansu Industrial Co., Ltd. Its purity is ≥98%, and it is a fine powder after grinding through a 100 mesh sieve. Industrial grade borax decahydrate ($Na_2B_4O_7{\cdot}10\ H_2O$) is a white granular crystal with a purity of ≥95%. SF obtained from China Henan Porun Casting Material Co., Ltd., having a SiO_2 content ≥95% was used. Standard sand was used after screening to remove particles below 0.3 mm, and its fineness modulus was 2.93. The steel fiber was a copper-coated fiber with a diameter of 0.22 mm and a length of 13 mm. The chemical compositions of MgO and SF are shown in Table 1, and the particle size distribution curve is shown in

Table 1
Chemical composition of MgO and SF (wt%).

Raw material	MgO	SiO_2	Fe_2O_3	Al_2O_3	CaO	LOI
Magnesia	94.33	2.42	0.44	0.38	1.65	0.37
SF	0.22	95.36	0.25	0.49	1.61	0.17

LOI: loss on ignition

Fig. 1. The average particle size of MgO and SF is 20.8 μm and 1.28 μm respectively, and the average particle size of SF is much smaller than that of MgO.

2.2. Mix proportions

MAPC is a mixture of MgO, ADP, and $Na_2B_4O_7{\cdot}10\ H_2O$, and was used to prepare UHPC, fixing the total amount of cementing material and some key parameters (See Table 2). The ratio of MgO to ADP (M/P) was 3.5 and the ratio of $Na_2B_4O_7{\cdot}10\ H_2O$ to MgO (B/M) was 0.06. Meanwhile, the ratio of sand to cement (S/C) was 0.8 and that of water to cement (W/C) was 0.12. SF was used to replace 5%, 10%, and 15% of the binder (MgO+ADP+$Na_2B_4O_7{\cdot}10\ H_2O$) mass, respectively, and steel fiber with a 2% volume fraction was incorporated.

2.3. Sample preparation

MgO, ADP, $Na_2B_4O_7{\cdot}10\ H_2O$, SF, and sand were poured into the cement mortar mixer and were dry mixed for 30 s. Water was then added and stirred for 2 min. Then, steel fibers were added to the mixture and stirred continuously for 2–3 min. The prepared MAPC-UHPC mixture was quickly poured into a steel mold with a size of 40×40×160 mm, placed on a shaking table for 30 s, and molded under natural indoor conditions. Samples were demolded after 3 h, and cured at (20±2) ℃ and (50±5)% RH until the test age. The MAPC-UHPC preparation and testing process is shown in Fig. 2.

2.4. Test methods

2.4.1. Fresh properties

MAPC-UHPC without steel fiber was used to test the fluidity. The well-mixed MAPC-UHPC without steel fiber was quickly poured into the cone mold and the cone lifted in the vertical direction. Then, the flow table was dropped 25 times, and the spread diameter of the mixture was measured according to GB/T 8077–2012.

MAPC-UHPC paste was used to measure the setting time according to ASTM C191. Timing from the beginning of water mixing, close to the initial setting every 15 s measured. Due to the fast MAPC-UHPC hardening, and the short interval between the initial and final setting times, the initial setting time was used to characterize the MAPC-UHPC setting time.

2.4.2. Strength

The flexural (40×40×160 mm, 50 N/s) and compressive (40×40×40 mm, 2.4 kN/s) strengths of the MAPC-UHPC samples at 6 h, 3 d, and 28 d were determined using the integrated compression and folding machine of cement mortar according to GB/T17671–2021.

2.4.3. Microstructure

MAPC-UHPC specimens were cured to the test age, soaked in anhydrous ethanol for 24 h, hand-ground in an agate mortar through a 200-mesh sieve, and finally vacuum dried for 48 h to seal for XRD and TG testing. The hydration products were qualitatively analyzed by XRD. The Empyrean X-ray diffractometer of Panaco in the Netherlands was used to scan 5°–65° steps at 2°/min under the conditions

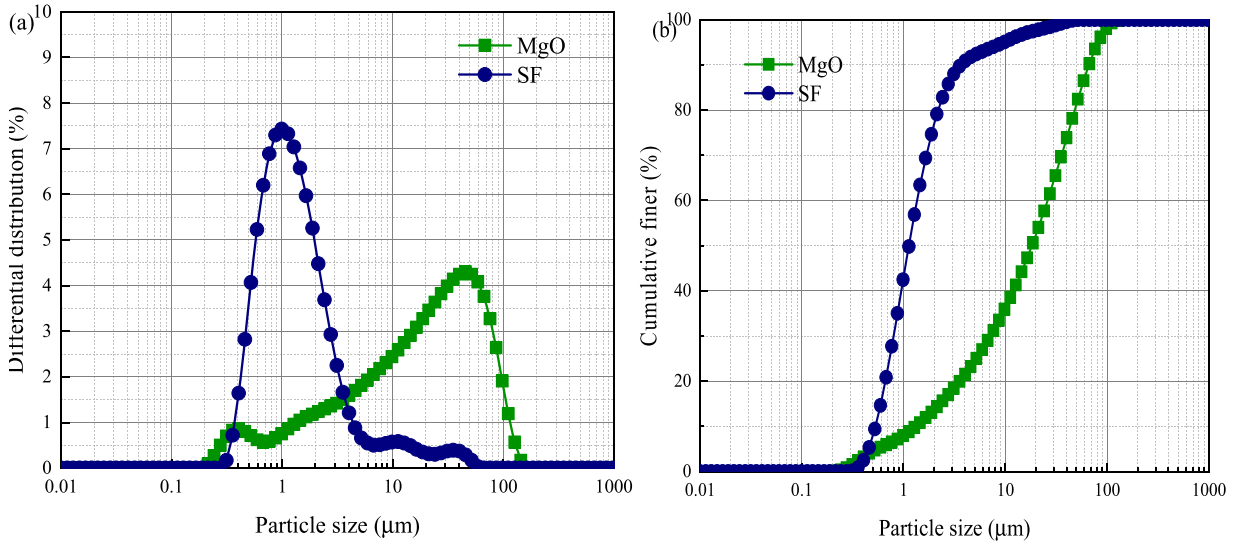


Fig. 1. MgO and SF particle size distributions: particle size distribution (a) and cumulative distribution (b).

Table 2
Mix ratio of MAPC-UHPC.

Mixture	Binder constituents (wt%)				Sand (wt%)	Steel fiber (vol%)	M/P	B/M	S/C	W/C
	MgO	ADP	$Na_2B_4O_7{\cdot}10\ H_2O$	SF						
SF0	844	241	51	0	909	2	3.5	0.06	0.8	0.12
SF5	802	229	48	57	909	2	3.5	0.06	0.8	0.12
SF10	759	217	46	114	909	2	3.5	0.06	0.8	0.12
SF15	717	205	43	171	909	2	3.5	0.06	0.8	0.12

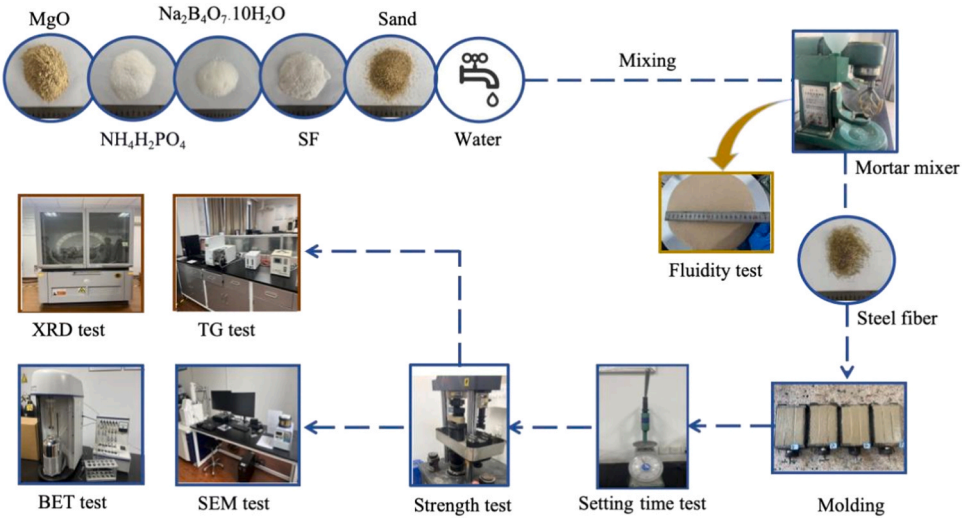


Fig. 2. MAPC-UHPC preparation and testing process.

of CuKα radiation generation at 40 mA and 40 kV and the step length at 0.02°2θ. TG test is mainly used for quantitative analysis of sample hydration products. A TG/DTA6300 synchronous thermal analyzer was used to test at a rate of 10 ℃/min from room temperature to 980 ℃ in N_2 environment.

The MAPC-UHPC sample was broken, the middle 2–5 mm fragments were put into anhydrous ethanol to stop hydration, and then the specimens were vacuum-dried and sealed for the test of microscopic morphology and pore structure. SU3800 scanning electron microscope (SEM) was used to photograph the morphology of the sample, and TriStar II 3020 specific surface area meter was used to measure the pore distribution of the specimen.

3. Results and discussion

3.1. Workability

The measured fluidity of the MAPC-UHPC mixture without the steel fiber is shown in Fig. 3. Fig. 4 shows the effect of SF on the fluidity and setting time of the MAPC-UHPC mixture. With an increase in the SF content, the mixture fluidity gradually increased. When 5% SF was added, the mixture fluidity was 231 mm, which was significantly higher than that of the control sample (208 mm), and the increase in sample fluidity gradually slowed down as the SF content continued to increase. When 10% SF was added, the mixture fluidity was 245 mm. When 15% SF was added, the sample fluidity reached a maximum of 246 mm, indicating that SF has a positive effect on the improvement of the mixture fluidity. This is mainly attributed to the smooth surface of the spherical shape of SF, which can play a good role in the "ball effect" and reduce the frictional resistance among the irregular MgO particles [32–35]. In addition, the average particle size of SF is 1.28 μm, which enables it to uniformly fill the voids between the MAPC particles and the hydration products. This forms a good micrograding effect and improves the packing density, which is conducive to the release of more free water, thus improving the fluidity of the mixture [36].

The setting time of the MAPC-UHPC paste increased with the increase in SF content. The setting time of the 15% SF paste reached a maximum of 8.5 min, which is 54.5% longer than the setting time of 5.5 min for the control group. The hydration reaction of the silicate phase in spherical SF is low, and it is difficult to participate in the violent acid-base reaction during the initial stage of hydration [37]. Meanwhile, the pH value also affects the setting time of the MPC paste [38]. With an increase in the SF content, the pH value of the sample gradually decreases, resulting in a prolonged setting time [32]. In addition, SF replaces MAPC, diluting the concentration of MgO and reducing the heat release rate of the hydration reaction, effectively alleviating the sharp temperature rise caused by MgO hydration. This delays the hydration rate and results in fewer hydration products being formed in the initial stage of hydration [39].

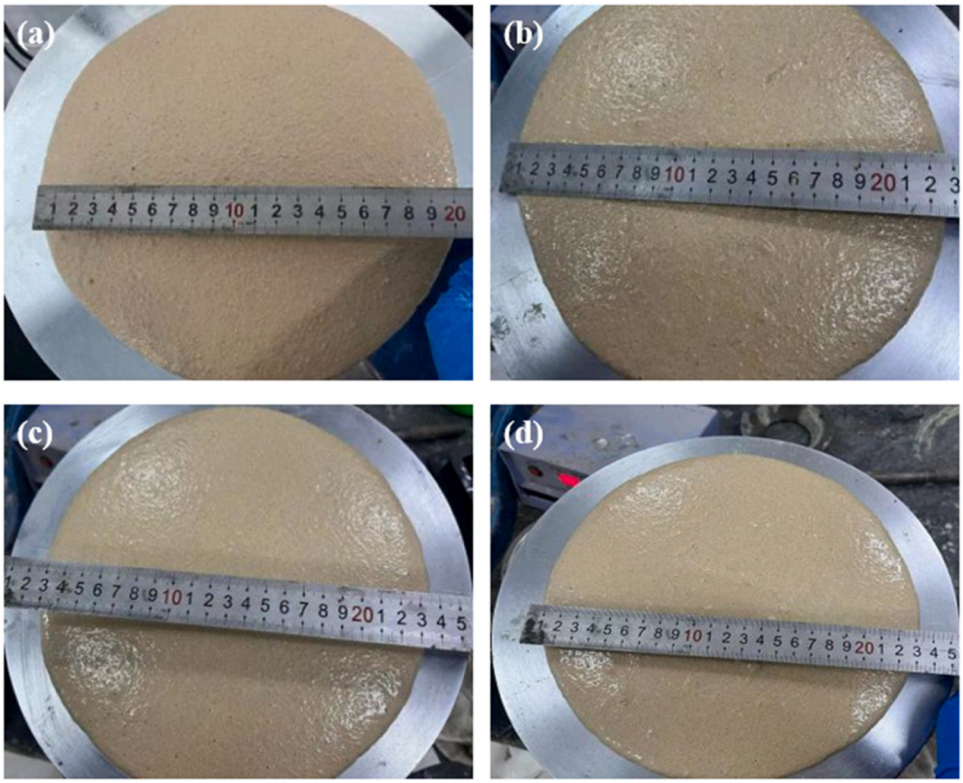


Fig. 3. Measured fluidity of MAPC-UHPC without steel fiber: SF0 (a), SF5 (b), SF10 (c), and SF15 (d).

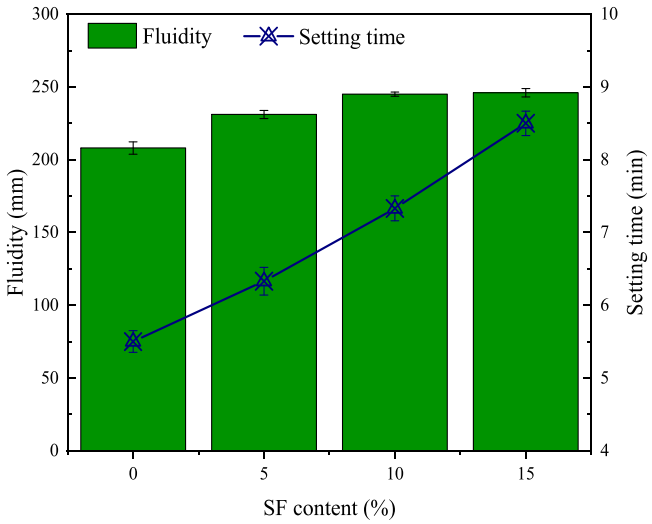


Fig. 4. Effect of SF on MAPC-UHPC fluidity and setting time.

Therefore, SF substitution prolonged the setting time of MAPC-UHPC by changing the pH value as well as its dilution effect.

3.2. Strength

The influence of SF at different ages on the compressive strength of the MAPC-UHPC samples is shown in Fig. 5(a). When the age was 6 h, the compressive strength of MAPC-UHPC first increased and then decreased with an increase in the SF content. The compressive strengths of 5%, 10%, and 15% SF-modified samples were 106.4, 120.3, and 103.6 MPa, respectively, which were

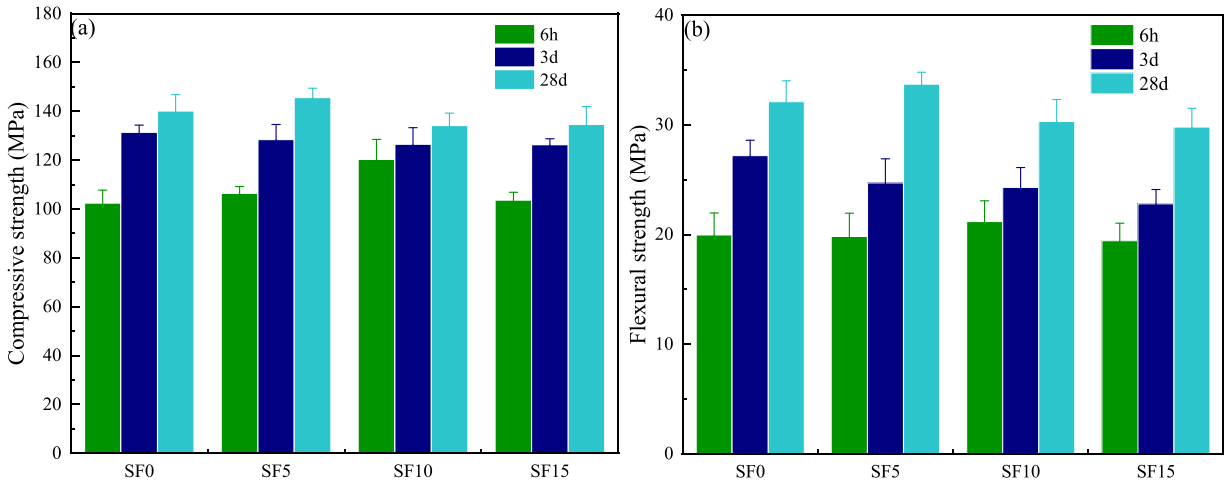


Fig. 5. Influence of SF on the compressive (a) and flexural strengths (b) of the MAPC-UHPC sample.

increased by 3.9%, 17.5%, and 1.2% compared with 102.4 MPa of the control group in sequence. This indicates that the addition of 10% SF has an obvious positive effect on the 6-h compressive strength of the MAPC-UHPC sample. At the age of 3 d, the compressive strength of MAPC-UHPC gradually decreased with increasing SF content, but the decrease was not obvious. However, at the age of 28 d, the compressive strength of the sample added with 5% SF was the highest, which was 5.4 MPa higher than that of the control specimen of 140.2 MPa. The influence of SF at different ages on the flexural strength of MAPC-UHPC is shown in Fig. 5(b). At the age of 6 h, the flexural strength of the MAPC-UHPC sample mixed with 10% SF was close to that of SF0 sample. The changing trends of flexural strengths of the MAPC-UHPC sample at the age of 3 d and 28 d were similar to the compressive strength at the same age. At 28 d, the flexural strength of SF0 was 32.1 MPa, and the flexural strength of 5% SF-modified samples increased to 33.7 MPa, whereas the flexural strengths of 10% and 15% SF-modified samples decreased to 30.3 and 29.8 MPa, respectively.

The strength of MAPC-UHPC was improved by adding proper SF. SF is fine and has a smooth and round surface. Its microaggregate effect can fill pores and cracks, and improve particle composition and fluidity [40]. SF can also exert a nucleation effect, promote the hydration reaction of MAPC-UHPC, and form more hydration products [41]. In addition, SF may rehydrate with unreacted MgO to produce other products such as $MgSiO_3$ [42], which also helps to improve the compactness of the sample. In addition, MgO and ADP have high reactivity, the use of SF to replace MAPC, the total cementing material unchanged, reduce the overall system heat release, and then affect the early strength development. However, compared with the high reactivity of MgO, the addition of excessive SF also weakens the adhesion inside the sample, resulting in a decline in strength [37].

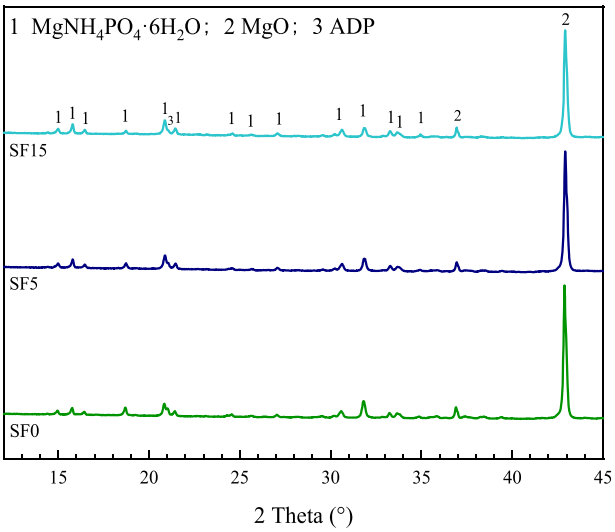


Fig. 6. XRD pattern of MAPC-UHPC doped with SF.

3.3. Microscopic analysis

3.3.1. XRD analysis

Fig. 6 shows the diffraction patterns of specimens of SF0, SF5, and SF15 at 28 d of age. The main hydration product for both the plain and SF-doped MAPC samples is struvite. For SF0, there is a shoulder peak on the main peak of 21°, which indicates that there is still a small amount of residual ADP. This may adversely affect the compactness and strength of the MAPC-UHPC matrix. However, with an increase in the SF content, the residual ADP gradually disappeared, while at the same time, the characteristic peak intensity of MgO gradually decreased. This is because SF replaces cement, resulting in a gradual decrease in the ADP and MgO contents, and the system has more water available for the reaction between the two components. Previous studies have demonstrated that there is hydrolysis of MgO to $Mg(OH)_2$ to react with reactive SiO_2 to form $MgSiO_3$ in MAPC and MKPC [42–44]. Because only a small amount of $MgSiO_3$ was formed, which was below the detection limit of the X-ray diffractometer, no obvious $MgSiO_3$ diffraction peaks were observed. $MgSiO_3$ is an M-S-H gel [45], which improves the solid-phase bonding of MAPC and, in turn, contributes to the strength of MAPC-UHPC.

3.3.2. TG-DTG analysis

Fig. 7 shows the TG-DTG curves of the samples of SF0, SF5, and SF15 at 28 d of age, and the corresponding TGA calculations are shown in Table 3. Compared with SF0, no new weight loss peaks were found in the TG-DTG plots for SF5 and SF15. In the MPC system, the decreasing process of the TG curves mainly consists of two phases [46,47]. The first phase is the loss of water of crystallization and the release of ammonia at RT-200 °C, and the second phase is the loss of structural water and reconfiguration above 200 °C.

The mass loss of SF0, SF5, and SF15 mainly occurred in the range of RT-200 °C, that is, the dehydration decomposition of the main hydration product struvite and other hydration products, and the mass losses were 10.86%, 12.91%, and 11.40%, respectively (See Table 3). By comparing the mass loss and mass loss peak area of each sample below 200 °C, it was found that the mass loss first increased and then decreased with the increase in SF content. Because struvite is the main hydration product of MAPC, the content of struvite plays a crucial role in the strength development of MAPC-UHPC. In general, the higher the struvite content, the more beneficial the strength development [48]. Therefore, the incorporation of SF increased the mass loss of MAPC to some extent, indicating that the addition of SF could promote hydration to form more hydration products. This may explain the increase in strength of SF5 at 28 d, whereas SF15 has a smaller loss similar to that of SF0.

There were three significant decomposition peaks, which are about 60, 100, and 200 °C, respectively. The peak value at 60 °C is due to the decomposition of the intermediate reaction product of struvite [49], which could not be detected in the XRD pattern because of the low mass of the product. A significant decomposition peak occurred at 100 °C, mainly due to the thermal decomposition of struvite and other hydration products in their final form [50]. In addition, the peak around 200 °C is derived from the thermal decomposition of residual ADP [47,51]. The control group of SF0 had more unreacted ADP than SF5 and SF15, which is consistent with the XRD results. The presence of residual ADP may be related to the short stirring time and fast hardening speed. This leads to the failure of ADP to fully react into struvite, which may have an adverse effect on strength development. Under a constant free water content, the effective water to binder (MgO, ADP and $Na_2B4O_7{\cdot}10\ H_2O$) ratio can be increased by adding an appropriate amount of SF, which is conducive to the hydration reaction of the specimen. SF5 has the least amount of unreacted ADP, indicating that it has the most adequate reaction and the best effect on strength enhancement [49].

3.3.3. Pore structure

Fig. 8 shows the pore structure of the MAPC-UHPC sample doped with SF at the age of 28 d. In cement-based materials, the pore

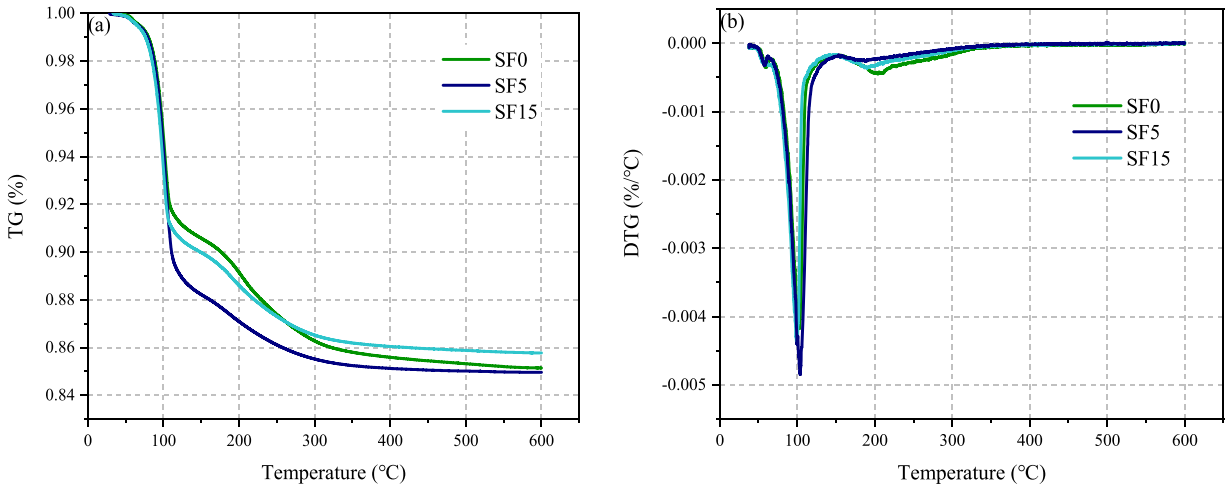


Fig. 7. TG-DTG of MAPC-UHPC doped with SF, (a) TG curves, and (b) DTG curves.

Table 3
TGA results for MAPC-UHPC doped with SF.

Group	RT-200 (℃)	200–600 (℃)	RT-600 (℃)
SF0	10.86%	4.00%	14.86%
SF5	12.91%	2.13%	15.04%
SF15	11.40%	2.82%	14.22%

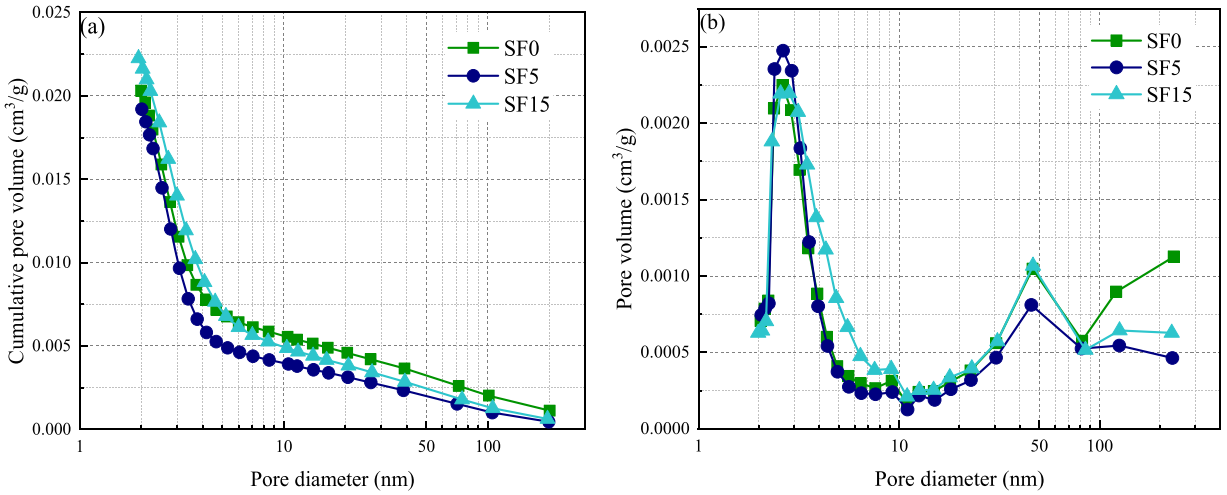


Fig. 8. Pore structure of MAPC-UHPC doped with SF: pore accumulation curve (a) and pore distribution curve (b).

structure can be generally divided into four categories [50,51]: gel pores (<10 nm), medium pores (10–50 nm), large pores (50–100 nm), and harmful pores (> 100 nm). The pore structure of the sample is mainly concentrated in gel pores below 10 nm, as shown in Fig. 8. The cumulative porosities of SF0, SF5, and SF15 were 0.020, 0.019, and 0.022 cm^3/g, respectively, which is consistent with the strength gain. The average pore diameter of SF0 was 3.41 nm, whereas that of SF5 and SF15 was 3.24 and 3.70 nm, respectively, indicating that the addition of 5% SF refined the pore structure of MAPC-UHPC [52]. The addition of excessive SF increased cumulative porosity and average pore size because the increase in the effective water-binder ratio led to greater porosity.

3.3.4. SEM analysis

Fig. 9 shows the microstructure of different MAPC-UHPC samples at 28 d. The microstructure of the SF0 matrix was mainly composed of unreacted MgO particles, sand particles, and the hydration product struvite, which has an irregular crystal morphology. The matrix microstructure of the SF5 sample doped with SF was similar to that of SF0, containing spherical SF particles. SF particles were mixed with hydration products and unreacted components to further densify the matrix microstructure. Fig. 10 shows the effect of SF on the 28-d microstructure of the ITZ in the MAPC-UHPC sample. The SF0 sample without SF added had a thin ITZ, as shown in Fig. 10(a). When 5% SF was added, the SF5 matrix was more closely connected to the aggregate, and the width of the ITZ was small, as presented in Fig. 10(b). Therefore, the addition of 5% SF not only improved the compactness of the matrix but also enhanced the performance of the ITZ, which promoted the MAPC-UHPC strength.

Fig. 11 shows the microstructure of the ITZ between the UHPC matrix and steel fiber at the age of 28 d. There were more pores around the steel fiber in the SF0 sample, as shown in Fig. 11(a). The addition of fiber may bring about a "wall effect", resulting in pores more easily clustered around the steel fiber, weakening the connection between the matrix and the steel fiber. Compared with SF0, the pores around the steel fibers in SF5 were smaller and less obvious, and the matrix was more closely connected with the steel fibers, as shown in Fig. 11(b). In addition, more residual matrix components adhered to the surface of the steel fiber in the SF5 sample, which indicates a better bonding property between the matrix and steel fiber.

4. Conclusions

In this study, MAPC was used to prepare UHPC with the characteristics of rapid hardening and high early-age strength, and the effect of SF on its mechanical properties and microstructure was studied. The following major conclusions can be drawn:

(1) Adding 5–15% SF increased MAPC-UHPC fluidity and setting time, and the effect was better with the increase in SF content. When the SF content was 15%, the fluidity and setting time of the UHPC mixture increased by 18.27% and 54.55% respectively, compared with the plain mixture.

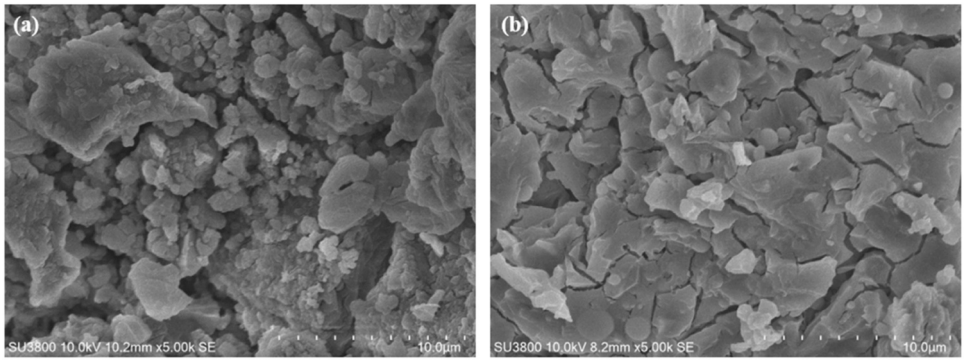


Fig. 9. SEM image of MAPC-UHPC matrix, (a) SF0 and (b) SF5.

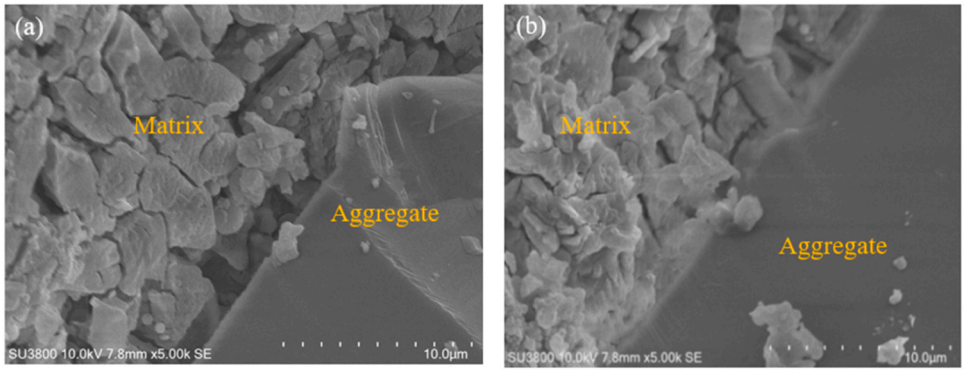


Fig. 10. SEM image of the ITZ between matrix and aggregate: SF0 (a) and SF5 (b).

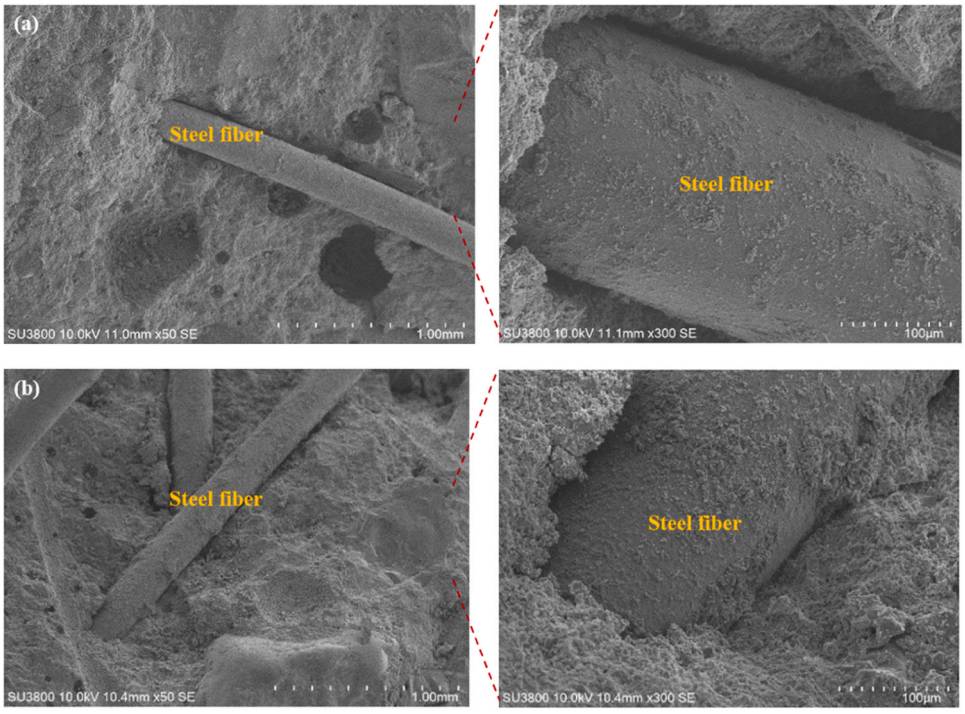


Fig. 11. SEM image of the ITZ between the matrix and steel fiber: SF0 (a) and SF5 (b).

(2) The 6-h compressive strength of MAPC-UHPC was greater than 100 MPa, which meets the needs of repair projects. Adding a small amount of SF improved the early strength of MAPC-UHPC and also had a positive effect on long-term strength. When 5% SF was used, the 6-h and 28-d compressive strengths of MAPC-UHPC increased by 3.91% and 3.86% respectively compared with the plain sample.
(3) Microscopic experimental analysis showed that adding an appropriate amount of SF promoted hydration and generated more hydration products (mainly struvite). Adding 5% SF reduced the porosity of MAPC-UHPC and refined its pore structure. Meanwhile, SF also densified the UHPC matrix microstructure and reduced ITZ between the matrix and aggregate/steel fibers.

Above all, SF-substituted MAPC-UHPC can be used for rapid repair purposes and also pave the way for a shortened production period and lowered energy costs in prefabricated elements in comparison with Portland cement-based UHPC. The durability properties of MAPC-UHPC, however, should be examined comprehensively in future studies.

Funding

This work was supported by Natural Science Foundation of Zhejiang Province (Grant No. LY20E020006).

CRediT authorship contribution statement

Zhi-hai He: Conceptualization, Funding acquisition, Writing – review & editing. **Yuan-yuan Jiang**: Formal analysis, Investigation. **Jin-yan Shi**: Methodology, Writing – review & editing. **Jihui Qin**: Validation, Visualization. **De-e Liu**: Validation, Writing - original draft. **Çağlar Yalçınkaya**: Validation, Writing - original draft. **Yi-feng He**: Conceptualization, Funding acquisition.

Declaration of Competing Interest

None.

Data Availability

Data will be made available on request.

References

[1] M. Dahal, S. Park, S. Pyo, A modified approach for measuring the air permeability of ultra-high performance concrete (UHPC) under vacuum conditions, Constr. Build. Mater. 401 (2023) 132933.
[2] C. Jithendra, S. Elavenil, Effects of silica fume on workability and compressive strength properties of aluminosilicate based flowable geopolymer mortar under ambient curing, Silicon 12 (8) (2020) 1965–1974.
[3] Q. Ding, J. Gong, G. Zhang, et al., Preparation and properties of HUHPC with low shrinkage and high impact resistance, KSCE J. Civ. Eng. 27 (8) (2023) 3430–3440.
[4] W.P. Xue, C. Twenda, M.S. Alam, et al., Experimental study on seepage characteristics and stress sensitivity of desulfurization gypsum based concrete under triaxial stress, J. Mater. Res. Technol. 24 (2023) 6425–6437.
[5] Mohamed Amin, et al., Influence of recycled aggregates and carbon nanofibres on properties of ultra-high-performance concrete under elevated temperatures, Case Stud. Constr. Mater. 16 (2022) e01063.
[6] Hongyan Chu, et al., Effects of steel chips on the microstructure, mechanical property, and durability of ultra-high-performance concrete with high elastic modulus, J. Build. Eng. 72 (2023) 106662.
[7] M.H. Akeed, S. Qaidi, H.U. Ahmed, et al., Ultra-high-performance fiber-reinforced concrete. Part IV: durability properties, cost assessment, applications, and challenges, Case Stud. Constr. Mater. 17 (2022) e01271.
[8] J. Du, W. Meng, K.H. Khayat, et al., New development of ultra-high-performance concrete (UHPC), Compos. Part B Eng. 224 (9)) (2021) 109220.
[9] Ibrahim Y. Hakeem, et al., Properties of sustainable high-strength concrete containing large quantities of industrial wastes, nanosilica and recycled aggregates, J. Mater. Res. Technol. 24 (2023) 7444–7461.
[10] P. Shen, L. Lu, Y. He, et al., The effect of curing regimes on the mechanical properties, nano-mechanical properties and microstructure of ultra-high performance concrete, Cem. Concr. Res. 118 (2019) 1–13.
[11] R. Yu, P. Spiesz, H.J.H. Brouwers, Mix design and properties assessment of ultra-high performance fibre reinforced concrete (UHPFRC), Cem. Concr. Res. 56 (2014) 29–39.
[12] S. Fan, B. Chen, Experimental study of phosphate salts influencing properties of magnesium phosphate cement, Constr. Build. Mater. 65 (2014) 480–486.
[13] Y. Li, Y. Li, T. Shi, et al., Experimental study on mechanical properties and fracture toughness of magnesium phosphate cement, Constr. Build. Mater. 96 (2015) 346–352.
[14] Y. Jiang, M.R. Ahmad, B. Chen, Properties of magnesium phosphate cement containing steel slag powder, Constr. Build. Mater. 195 (2019) 140–147.
[15] Y. Wei, C. Song, B. Chen, et al., Experimental investigation on two new corn stalk biocomposites based on magnesium phosphate cement and ordinary Portland cement, Constr. Build. Mater. 224 (2019) 700–710.
[16] Z. Jiang, C. Qian, Q. Chen, Experimental investigation on the volume stability of magnesium phosphate cement with different types of mineral admixtures, Constr. Build. Mater. 157 (2017) 10–17.
[17] W.P. Xue, T. Min, M.S. Alam, et al., Evolution characteristics and mechanism of concrete performance under water pressure environment: a comprehensive review, Struct. Concr. 24 (2023) 6338–6369.
[18] Mohamed Amin, et al., Investigation of the physical mechanical properties and durability of sustainable ultra-high performance concrete with recycled waste glass, Sustainability 15 (4) (2023) 3085.
[19] Hongyan Chu, et al., Feasibility of producing ultra-high performance concrete with high elastic modulus by steel chips: An experimental study, Constr. Build. Mater. (375s) (2023) 130964.
[20] F. Qiao, C.K. Chau, Z. Li, Property evaluation of magnesium phosphate cement mortar as patch repair material, Constr. Build. Mater. 24 (5) (2010) 695–700.
[21] J. Qin, H. Zhu, Z. He, et al., Recycling of water treatment sludge into magnesium potassium phosphate cement component by a combination of silica fume, J. Build. Eng. 51 (2022) 104308.

[22] L.J. Gardner, C.L. Corkhill, S.A. Walling, et al., Early age hydration and application of blended magnesium potassium phosphate cements for reduced corrosion of reactive metals, Cem. Concr. Res. 143 (2021) 106375.
[23] A.J. Wang, J. Zhang, J.M. Li, et al., Effect of liquid-to-solid ratios on the properties of magnesium phosphate chemically bonded ceramics, Mater. Sci. Eng.: C. 33 (5) (2013) 2508–2512.
[24] B. Chen, X.Y. Yang, N. Liu, Experimental research on the properties of modified MPC, Adv. Mater. Res. 450-451 (4)) (2012) 796–799.
[25] M. Gao, B. Chen, L. Lang, et al., Influence of silica fume on mechanical properties and water resistance of magnesium-ammonium phosphate cement, J. Mater. Civ. Eng. 32 (3) (2020) 04019368.
[26] J. Qin, F. Dai, H. Ma, et al., Development and characterization of magnesium phosphate cement based ultra-high performance concrete, Compos. Part B: Eng. 234 (2022) 109694.
[27] W. Tian, Y. Liu, M. Wang, et al., Performance and economic analyses of low-energy ohmic heating cured sustainable reactive powder concrete with dolomite powder as fine aggregates[J], J. Clean. Prod. 329 (2021) 129692.
[28] K. Yang, G. Long, Z. Tang, et al., Insight into the flexural characteristics of rapid hardening ultra-high performance concrete (RH-UHPC) incorporating CSH seeds using acoustic emission technology, Constr. Build. Mater. 408 (2023) 133632.
[29] J.Y. Zhu, F.X. Chen, X.Q. Dai, et al., Development of a novel ultra-high performance concrete (UHPC) suitable for underwater operation: Design and performance evaluation, J. Build. Eng. (2023) 107030.
[30] H. Zhou, X. Qi, C. Ma, et al., Effect and mechanism of composite early-strength agents on sulfoaluminate cement-based UHPC, Case Stud. Constr. Mater. 18 (2023) e01768.
[31] A.A.J. Ghanim, M. Amin, A.M. Zeyad, et al., Effect of modified nano-titanium and fly ash on ultra-high-performance concrete properties, Struct. Concr. 24 (5) (2023) 6815–6832.
[32] X. Xu, X. Lin, X. Pan, et al., Influence of silica fume on the setting time and mechanical properties of a new magnesium phosphate cement, Constr. Build. Mater. 235 (2020) 117544.
[33] Ahmed M. Tahwia, Gamal M. Elgendy, Mohamed Amin, Mechanical properties of affordable and sustainable ultra-high-performance concrete, Case Stud. Constr. Mater. 16 (2022) e01069.
[34] Ibrahim Y. Hakeem, et al., Using a combination of industrial and agricultural wastes to manufacture sustainable ultra-high-performance concrete, Case Stud. Constr. Mater. 19 (2023) e02323.
[35] Hongyan Chu, et al., Mechanical properties and microstructure of ultra-high-performance concrete with high elastic modulus, Constr. Build. Mater. 335 (2022) 127385.
[36] Y. Zhang, S. Wang, B. Zhang, et al., A preliminary investigation of the properties of potassium magnesium phosphate cement-based grouts mixed with fly ash, water glass and bentonite, Constr. Build. Mater. 237 (2020) 117501.
[37] Y. Liu, B. Chen, B. Dong, et al., Influence mechanisms of fly ash in magnesium ammonium phosphate cement, Constr. Build. Mater. 314 (2022) 125581.
[38] Y. Li, T. Shi, B. Chen, Experimental study of dipotassium hydrogen phosphate influencing properties of magnesium phosphate cement, J. Mater. Civ. Eng. 28 (4) (2015) 04015170.
[39] D. Dong, Y. Huang, Y. Pei, et al., Effect of spherical silica fume and fly ash on the rheological property, fluidity, setting time, compressive strength, water resistance and drying shrinkage of magnesium ammonium phosphate cement, J. Build. Eng. 63 (2023) 105484.
[40] Hakeem, Y. Ibrahim, et al., Effects of nano-silica and micro-steel fiber on the engineering properties of ultra-high performance concrete, Struct. Eng. Mech. 82 (3) (2022) 295–312.
[41] Ibrahim Y. Hakeem, et al., Properties of sustainable high-strength concrete containing large quantities of industrial wastes, nanosilica and recycled aggregates, J. Mater. Res. Technol. 24 (2023) 7444–7461.
[42] M.R. Ahmad, B. Chen, Effect of silica fume and basalt fiber on the mechanical properties and microstructure of magnesium phosphate cement (MPC) mortar, Constr. Build. Mater. 190 (2018) 466–478.
[43] D.D. Zheng, T. Ji, C.Q. Wang, et al., Effect of the combination of fly ash and silica fume on water resistance of magnesium–potassium phosphate cement, Constr. Build. Mater. 106 (2016) 415–421.
[44] Mana Alyami, et al., Effect of agricultural olive, rice husk and sugarcane leaf waste ashes on sustainable ultra-high-performance concrete, J. Build. Eng. 72 (2023) 106689.
[45] Y. Liu, B. Chen, Z. Qin, Effect of nano-silica on properties and microstructures of magnesium phosphate cement, Constr. Build. Mater. 264 (2020) 120728.
[46] B. Lothenbach, B. Xu, F. Winnefeld, Thermodynamic data for magnesium (potassium) phosphates, Appl. Geochem. 111 (2019) 104450.
[47] B. Tansel, G. Lunn, O. Monje, Struvite formation and decomposition characteristics for ammonia and phosphorus recovery: A review of magnesium-ammonia-phosphate interactions, Chemosphere: Environ. Toxicol. risk Assess. 194 (2018) 504–514.
[48] Y. Tan, H. Yu, Y. Li, et al., Magnesium potassium phosphate cement prepared by the byproduct of magnesium oxide after producing Li_2CO_3 from salt lakes, Ceram. Int. 40 (8) (2014) 13543–13551.
[49] B. Xu, H. Ma, H. Shao, et al., Influence of fly ash on compressive strength and micro-characteristics of magnesium potassium phosphate cement mortars, Cem. Concr. Res. 99 (2017) 86–94.
[50] L. Yue, S. Tongfei, C. Bing, L. Yaqiang, Performance of magnesium phosphate cement at elevated temperatures, Constr. Build. Mater. 91 (2015) 126–132.
[51] Y. Liu, B. Chen, Z. Qin, et al., Experimental research on properties and microstructures of magnesium-iron phosphate cement, Constr. Build. Mater. 257 (2020) 119570.
[52] Hongyan Chu, et al., An approach of producing ultra-high-performance concrete with high elastic modulus by Nano-Al_2O_3: a preliminary study, Materials 15 (22) (2022) 8118.